Gold Catalysts Supported on Cerium–Gallium Mixed Oxide for the Carbon Monoxide Oxidation and Water Gas Shift Reaction

Topics in Catalysis

ISSN 1022-5528
Volume 54
Combined 1-4

Top Catal (2011) 54:201-209
DOI 10.1007/
s11244-011-9653-6

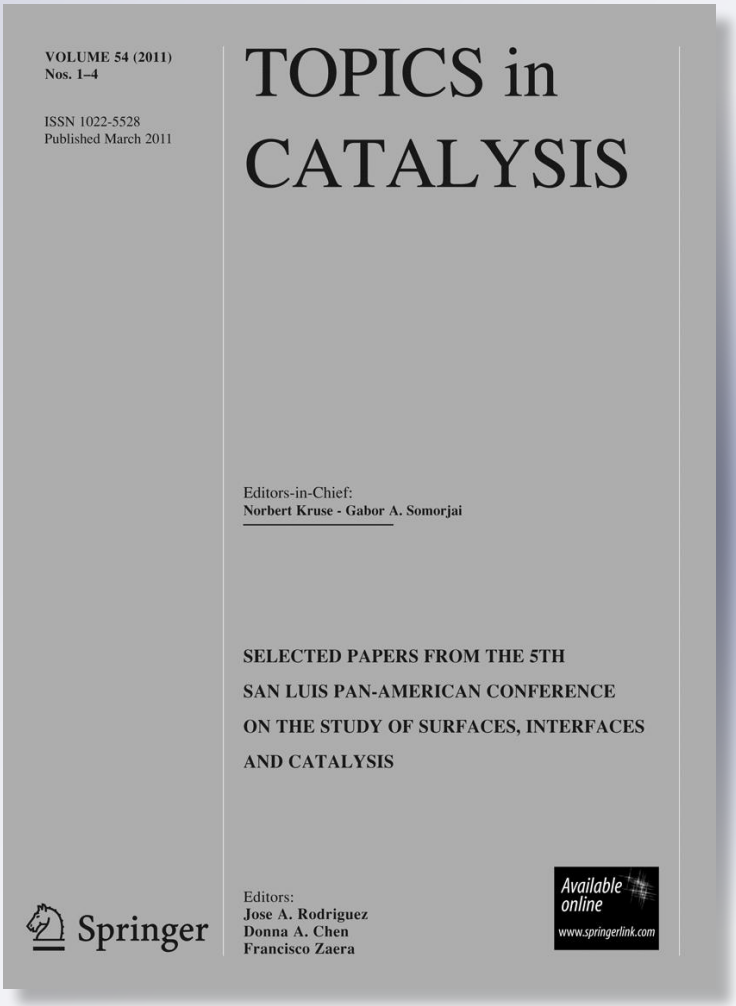

Springer

Top Catal (2011) 54:201–209
DOI 10.1007/s11244-011-9653-6

ORIGINAL PAPER

Gold Catalysts Supported on Cerium–Gallium Mixed Oxide for the Carbon Monoxide Oxidation and Water Gas Shift Reaction

Julia Vecchietti · Sebastián Collins · Juan José Delgado · Małgorzta Małecka · Eloy del Rio · Xiaowei Chen · Serafin Bernal · Adrian Bonivardi

Published online: 28 January 2011

Abstract The synthesis, characterization and catalytic properties of gold supported on ceria, gallia and a cerium–gallium mixed oxide were investigated. The nanostructural characterization of the cerium–gallium support (nominal atomic composition Ce80Ga20) showed that gallium(III) cations are homogenously distributed into the ceria matrix by substituting cerium(IV) cations of the fluorite-type structure of ceria. Au was added to the supports by the deposition–precipitation method using urea. High Au dispersions were achieved for all the fresh materials ($D > 60\%$). The CO oxidation and the water gas shift (WGS) reaction were tested on the whole set of catalysts. All the supported-gold catalysts showed high activity for the CO oxidation reaction. However, those containing gallium in their formulation deactivated due to gold particle sinterization. $Au(2\%)/CeO_2$ was the most active material for the WGS reaction, and the Au(2%)/Ce80Ga20 was as active as a Au(3%)/Ce68Zr32 catalyst for CO oxidation, and even more active than the reference catalyst of the World Gold Council, $Au(2\%)/TiO_2$.

Keywords Au/CeO_2 · Au/Ga_2O_3 · Au/Ce–Ga–O · WGS · PROX · Hydrogen purification

J. Vecchietti · S. Collins · A. Bonivardi (✉)
Instituto de Desarrollo Tecnológico para la Industria Química, UNL-CONICET, Güemes 3450, 3000 Santa Fe, Argentina
e-mail: abonivar@santafe-conicet.gov.ar

J. J. Delgado · M. Małecka · E. del Rio · X. Chen · S. Bernal
Dpto. de Ciencias de los Materiales, Ingeniería Metalúrgica y Química Inorgánica, Facultad de Ciencias, Universidad de Cádiz, 11510 Puerto Real, Spain

1 Introduction

One of the scenarios of the global energy market projections for 2100 indicates that 50% will correspond to hydrogen [1]. The transition between technologies based on oil and the ones using hydrogen as an energy source, will be slow and gradual, because of the lack of a massive infrastructure for transport and storage of gaseous hydrogen, and of the high cost for its direct production [2–4]. It is therefore considered reasonable the use of H_2 "carriers", such as hydrocarbons and alcohols, for application in fuel cells, in particular those based on polymeric membranes (PEMFC) [2–5] which are expected to be used in transportation and lightweight portable devices.

Conventionally, alcohols or hydrocarbons are transformed by steam reforming into a gaseous mixture that includes mainly CO, CO_2, H_2 and H_2O (called "synthesis gas" in the case of hydrocarbons) [1]. This implies the presence of significant CO concentrations in the output stream of the reformer, which should be decreased below 50 ppm, otherwise the Pt anode of the PEMFC is poisoned. In technological terms, the purification train involves the presence of a water gas shift (WGS) unit and a preferential CO oxidation unit, in the presence of a large excess of hydrogen (PROX). Thus, there is in the literature a broad consensus to develop new catalysts for WGS and PROX to improve current hydrogen generators to feed the PEMFC [6, 7].

For those purposes, catalytic systems containing highly dispersed gold have received great interest in recent years. The most remarkable catalytic properties of supported gold were observed by Haruta et al. in 1987 [8–10] in CO oxidation bellow room temperature. Thus, these gold based systems have been considered promising candidates for

hydrogen purification through WGS and PROX, and for such catalytic applications, the optimum size of gold particles should be smaller than 5 nm [11–13]. Such particle sizes can be achieved by a careful control of the preparation conditions and storage of the catalysts [14].

Also, the nature of the support on which gold is dispersed plays a crucial role in determining the catalytic activity. The catalysts consisting of Au supported on CeO_2, and to a lesser extent on MO_X–CeO_2 mixed oxides, have received special attention [15, 16]. The relevance of these cerium based supports is primarily based on the remarkable oxygen storage capacity of these materials, which is linked to the creation, stabilization and diffusion of oxygen vacancies, especially in the oxide surface, due to the reversible redox property of the Ce^{4+}/Ce^{3+} pair. However, some authors have postulated that the deactivation of some of these cerium based systems can be attributed to the formation of strongly adsorbed carbonate species on ceria [16], and then, the tuning of the surface acid–basic properties could be envisage as an improvement in the stability of the catalysts.

To this last end, some of us have investigated the synthesis of Ce–Ga mixed oxides and have found that the gallium-doped ceria modifies the redox and acid–base properties of CeO_2. The formation of carbonates is inhibited at the same time that the redox properties are notoriously improved on doped ceria [17].

In this paper the results of the synthesis and characterization of a dispersed gold catalyst over a Ce–Ga support is presented. The catalytic performance of the CO oxidation and the WGS reaction is also evaluated on this new type of non conventional catalyst.

2 Experimental

2.1 Catalyst Preparation

$Ce(NO_3)_3{\cdot}6H_2O$ (99.99%, Sigma-Aldrich), $Ga(NO_3)_3{\cdot}9H_2O$ (99.999%, Sigma-Aldrich), $HAuCl_4{\cdot}3H_2O$ (≥49% Au, Sigma-Aldrich), urea (99.5%, Merk), and NH_4OH_{aq} (25% wt/v, Merck) were used for the preparation of the catalysts.

For the preparation of CeO_2 or Ce80Ga20 (nominal composition $Ce_{0.8}Ga_{0.2}O_{1.9}$) an aqueous solution of nitrate salts [0.17 M Ce or (0.15 M Ce + 0.04 M Ga), respectively] was slowly added (4 mL/min) to an aqueous solution of NH_4OH using a peristaltic pump to obtain 10 g of each calcined support. During the addition of the cations, the solution was vigorously stirred and the pH was kept at 8.5 by adding NH_4OH 12% wt/v to the suspension. Each solid was centrifugated and washed five times with water (ratio = 15 mL water/g dried support). Finally, each precursor was dried overnight at 120 °C.

The Ga_2O_3 was prepared by direct precipitation as previously described by some of us [18]. A solution of NH_4OH in ethanol (12% wt/v) was added drop wise to a solution 0.3 M $Ga(NO_3)_3$ in ethanol. After aging (4 h), the solid was separated by centrifugation and washed five times with ethanol (ratio = 15 mL ethanol/g dried support). Finally, the precipitate was dried under vacuum at 60 °C during 12 h.

Each dried material was calcined at 450 °C (2 °C/min, 5 h) in a glass tubular reactor under flowing 20% O_2/N_2 mixture (5 mL/min/g).

The method of deposition-precipitation with urea developed by Zanella et al. [19] was used to add 2% Au wt/wt to each calcined supports. Typically, 10 g of support was added to 1,000 mL of an aqueous solution of $HAuCl_4$ (10^{-3} M) and of urea (0.1 M). The suspension was vigorously stirred for 16 h at 80 °C. The resulting materials were centrifuged and washed with water until no chloride was detected in the washing solution. The obtained wet Au/support materials were dried under vacuum at 50 °C during 24 h. All the previous steps of gold impregnation, washing and drying were performed in the dark.

The dried supported Au catalysts (no further treatment) were stored in amber glass ampules closed under vacuum, and were further preserved at −18 °C before use.

2.2 Characterization

The Brunauer–Emmett–Teller surface area (S_{BET}) of each material, previously outgassed at 200 °C for 2 h under dynamic vacuum (base pressure = 1.33×10^{-4} Pa), was measured at −196 °C (LN2) using a Micromeritics ASAP-2020 apparatus. The X-ray diffraction patterns (XRD) were recorded using a Shimadzu XD-D1 diffractometer (Cu Kα radiation, 0.125°/min).

The redox property of the calcined supports was evaluated by temperature-programmed reduction with carbon monoxide (TPR-CO). The experiments were performed on 200 mg of sample placed in a U-shaped quartz reactor and the evolved gases were analyzed with a Pfeiffer Thermostar quadrupole mass spectrometer. The oxides were submitted to a cleaning procedure before running the TPR experiments [17]: (i) heating on 5% O_2/He (50 mL/min) at 500 °C (1 h), (ii) followed by cooling to 200 °C under the oxidizing mixture, and (iii) further to 25 °C in a flow of He (20 mL/min). Diluted carbon monoxide, 5% CO/He, was used as reducing agent (50 mL/min, 10 °C/min from 25 to 1,000 °C).

The mixed oxide support Ce80Ga20 and supported gold catalysts were investigated by electron microscopy using a Transmission Electron Microscope (TEM) model JEOL JEM-2010F equipped with a field emission gun and an acceleration voltage of 200 kV. The microscope was

operated in the high resolution mode (HRTEM) and dark-field scanning mode (HAADF-STEM). The structural resolution of the equipment in HRTEM mode is 0.19 nm while the probe used in STEM was 0.5 nm. The HAADF-STEM images provide an adequate contrast between the Au (Z = 79) and the cations of the support, Ce (Z = 58), Ga (Z = 31), Zr (Z = 40) and/or Ti (Z = 22) for accurate determination of the average size distribution of gold particles (the last two cations correspond to the reference samples described below). A minimum of 150 particles per sample were measured. To determine unequivocally the gold nanoparticles and to study the nanostructural homogeneity of the mixed oxide used as support, an energy dispersive spectrometer (EDS) in STEM mode was employed.

2.3 Catalytic Activity

The catalytic activity for CO oxidation of the samples was measured in a fixed bed glass tubular microreactor (i.d. = 7 mm). 25 mg of catalyst were diluted with 100 mg of quartz. The composition of the reaction mixture was 1% CO + 0.6% O_2 balanced with He (total flow = 100 mL/min). Light-off curves were performed from −40 to 145 °C (10 °C/min) keeping the temperature at 145 °C for 30 min and then cooling until the initial temperature (10 °C/min). The gases at the outlet of the reactor were analyzed with a mass spectrometer Pfeiffer Prisma model. Prior to the study of the catalytic activity, the dry supported Au catalysts were pretreated at 250 °C in an oxidizing atmosphere under flow of 5% O_2/He (60 mL/min) for 1 h and then under flow of He (60 mL/min) also during 1 h.

The effect of the pretreatment on CO oxidation was evaluated only over the Au/Ce80Ga20 catalyst. In addition to the previously described treatment (oxidizing atmosphere), the dry catalyst was also pretreated in: (i) reducing atmosphere under flow of 5% H_2/Ar (60 mL/min) at 200 °C (1 h) followed by flow of He (60 mL/min) for 1 h at the same temperature, and (ii) a sequential combination of oxidizing and then reducing atmosphere.

The catalytic activity of the catalysts for the water gas shift reaction (WGS) was measured in a fixed bed glass tubular microreactor (i.d. = 4 mm). 50 mg of catalyst were diluted with 100 mg of quartz. The reaction mixture composition was 1% CO + 1.9% H_2O balanced with He (total flow = 100 mL/min). Water was incorporated into the gas stream by means of a system consisting of a saturator and a condenser operated at 35 and 17 °C, respectively. To prevent condensation of water, all the pipelines were heated to 60 °C. The effluent gas composition was measured in a chromatograph Varian CP-4900 Micro GC with two TCD detectors. The columns used were Molecular Sieve 5 Å for the analysis of O_2, H_2 and CO, and CP-PoraPLOTQ for the analysis of CO_2 and H_2O. Catalytic activity measurements were performed in a range of 100–350 °C with steps of 50 °C (1 h). Prior to the catalytic performance measurements all the dry catalysts were pretreated under the oxidizing atmosphere as previously described.

3 Results and Discussion

3.1 Characterization

Table 1 shows the morphological characteristics of the supports used in this study. All the materials present moderate S_{BET} between 50 and 100 m^2/g, with mesoporuos structures (pore diameter >4 nm). The XRD results indicate that pure gallium oxide is present as the gamma phase and that cerium oxide and Ce80Ga20 show fluorite-type structure. Moreover, Fig. 1 shows the XRD patterns for the (111) diffraction peak of the fluorite-type structure of CeO_2, Ce80Ga20 and Au/Ce80Ga20 materials, and indicates that the deposition of gold did not affect the structure of the mixed oxide as revealed by the intensity, position and full-width-at-half-maximum of the signal. In general, both Table 1 and Fig. 1 suggest that the incorporation of the metallic function did not significantly modify any of those morphological and structural parameters of the supports.

As previously mentioned, the doping of ceria with Ga^{3+} was investigated by some of us [17]. Employing the same method of preparation described here, XRD and Raman spectroscopy results suggest that Ga^{3+} cations are incorporated in the lattice of the cerium dioxide, forming a mixed oxide [17].

To evaluate the nanostructural homogeneity of the Ce80Ga20 support composition, measurements by EDS mapping were performed. Figure 2a shows a HAADF-STEM micrograph of the Ce80Ga20 support and the

Table 1 Morphological and structural properties of the materials

Materials	S_{BET} (m^2/g)	V_P[a] (cm^3/g)	D_P[b] (nm)	Crystalline phase
CeO_2	62	0.16	9.6	Fluorite
Au/CeO_2	57	0.16	10.0	Fluorite
Ga_2O_3	77	0.10	3.8	Gamma
Au/Ga_2O_3	54	0.04	5.2	Gamma
Ce80Ga20	98	0.13	4.8	Fluorite
Au/Ce80Ga20	100	0.14	4.9	Fluorite

[a] Pore volume

[b] Pore average diameter

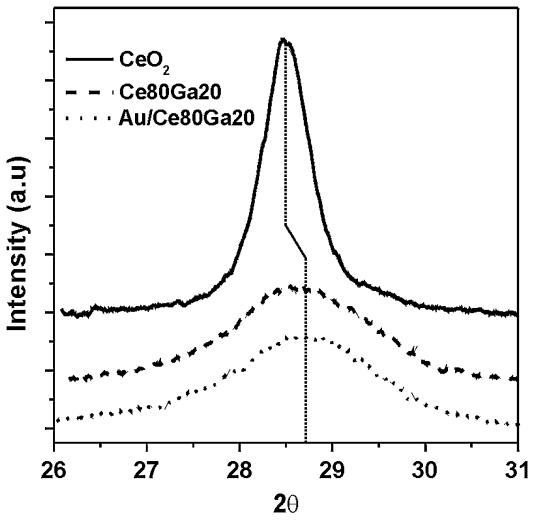

Fig. 1 XRD patterns of the (111) diffraction peak of the CeO_2, Ce80Ga20 and Au/Ce80Ga20 samples

elemental percentage composition of Ga and Ce for the different areas. The gallium content distribution is also shown in Fig. 2b. This figure shows that the Ce80Ga20 support is a homogeneous material, with a media composition close to the nominal Ce to Ga ratio equal to 80/20. It is important to notice that no segregated Ga_2O_3 or CeO_2 phases were detected. Moreover, Fig. 3 shows an image of HRTEM of the same support. The analysis of the digital diffraction patterns (DDPs) in the selected areas shows nanocrystals with 3.1 Å [1 1 1]F, 2.7 Å [2 0 0]F and 1.9 Å [2 2 0]F spacings, which are typical of the fluorite-type structure of CeO_2. Thus, we can conclude that the Ce80Ga20 support is essentially a solid solution.

The traces of the TPR-CO of the supports are depicted in Fig. 4. The reduction of the mixed oxide begins at approximately 100 °C, that is, 70 and 200 °C before the pure CeO_2 and Ga_2O_3, respectively. Moreover, the release of CO_2 was superior for the Ce80Ga20 sample than for any of the pure oxides. These features suggest that oxygen atoms are more labile in the gallium–cerium mixed oxide, since the Ce80Ga20 material is more reducible than any of the pure oxides. In other words, gallium cation incorporation into the lattice of ceria is able to induce the oxygen lost in a higher extension.

Figure 5 shows the particle size distributions of gold for each catalyst after the activation treatment in oxidizing atmosphere as determined by the analysis of the HAADF-STEM images. In all cases, these distributions are particularly narrow, with a mean metal particle diameter approximately equal to 1.5 nm, and gold crystallites larger than 3 nm are not observed. Then, the deposition-precipitation method of gold with urea led to a high metal dispersion (>60%), which is no affected by the type of support.

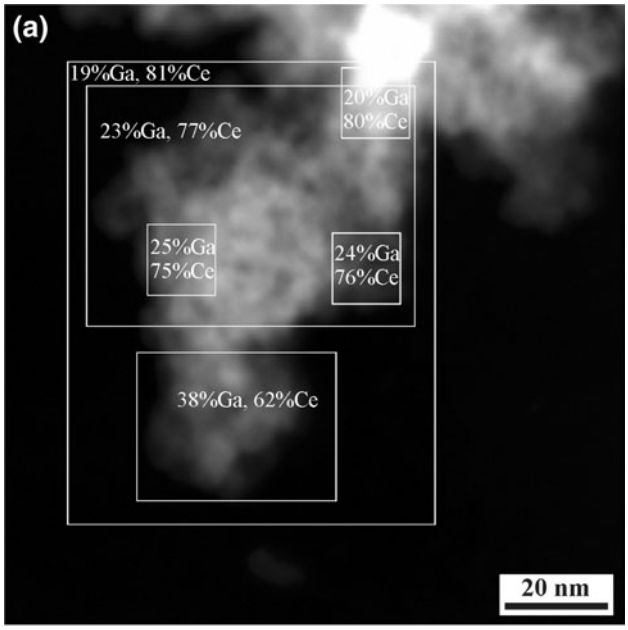

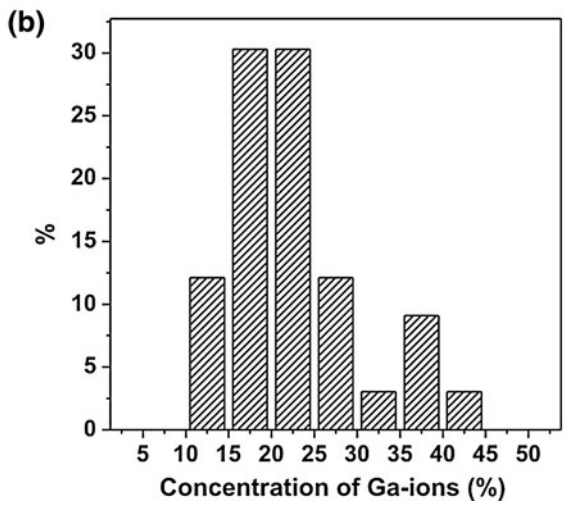

Fig. 2 **a** HAADF-STEM image of, and **b** distribution of Ga percentage in the Ce80Ga20 support

3.2 Catalytic Activity

3.2.1 Activation Treatment

It has been proposed that the preparation of gold catalyst by deposition-precipitation with urea involves the formation of a gold complex containing Au^{3+} at the surface of the support [20]. Thereupon, the materials must be submitted to an activation treatment to create catalytically active gold particles [21]. To determine an appropriate activation treatment of the catalysts, three pretreatment protocols were carried out under oxidizing, reducing and oxidizing-reducing atmosphere, as detailed in the Sect. 2. Afterwards,

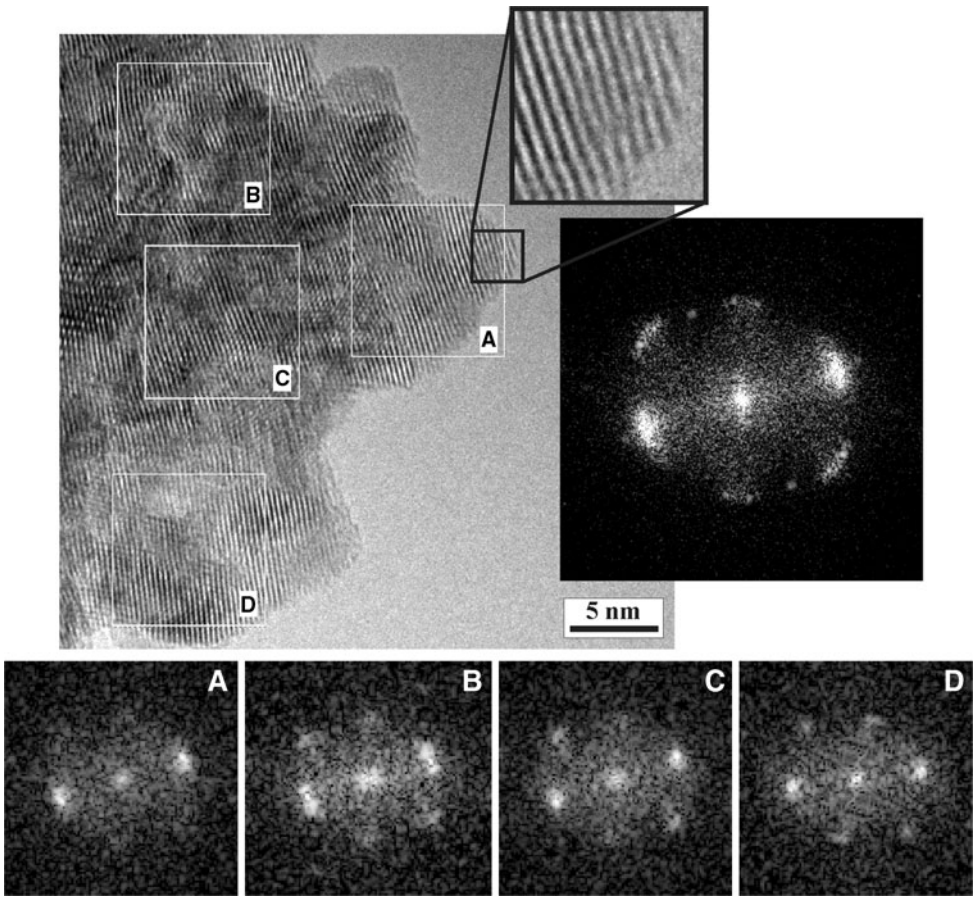

Fig. 3 HRTEM and DDPs patterns of the Ce80Ga20 support

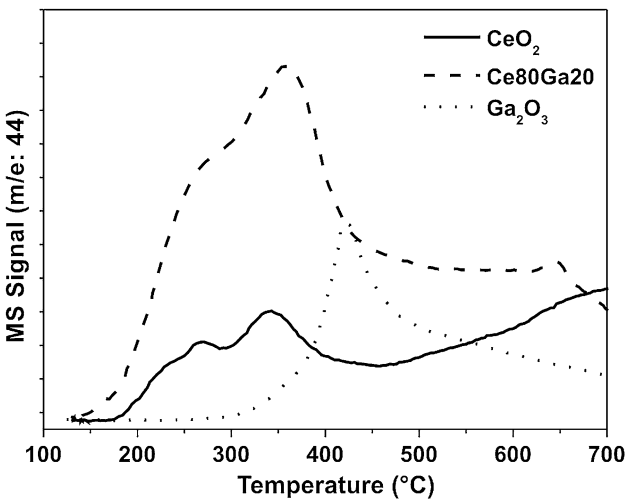

Fig. 4 Temperature-programmed reduction of cerium, gallium and cerium–gallium oxides, using carbon monoxide (TPR-CO)

the catalytic activity of the CO oxidation was used as a test reaction.

Figure 6 shows the light-off curves of CO conversion as a function of the activation treatment. First, it is clear that the Au/Ce80Ga20 catalyst without pretreatment was able to oxidize CO only from 100 °C, reaching a 100% of CO conversion at 145 °C (Fig. 6 curve a). In this case, the 50% of CO conversion was achieved at 110 °C—light-off temperature, T_{50}. Subsequently, during the cooling ramp the conversion curve shifted to lower values of temperature ($T_{50} = 70$ °C), which suggests that the catalyst was activated during the heating ramp under flowing reaction mixture.

Second, the light-off curves of CO conversion over a Au/Ce80Ga20 sample, which was previously pretreated under reduction [H_2(5%), 200 °C], and oxidation followed by reduction [O_2(5%), 250 °C + H_2(5%), 200 °C] conditions are almost identical, with a low temperature onset close to −30 °C and a $T_{50} \sim 40$ °C (see Fig. 6 curve b and c). These pretreatments were capable to generate a catalyst which was more active that the untreated one.

However, and finally, after the oxidizing treatment [O_2(5%), 250 °C] of the dried Au/Ce80Ga20 material, the catalyst showed the best performance, because it was active from −35 °C with a $T_{50} = 25$ °C (see Fig. 6 curve d).

Thus, the oxidizing activation treatment was chosen to study the catalytic behavior of our materials in both the CO oxidation and WGS reactions.

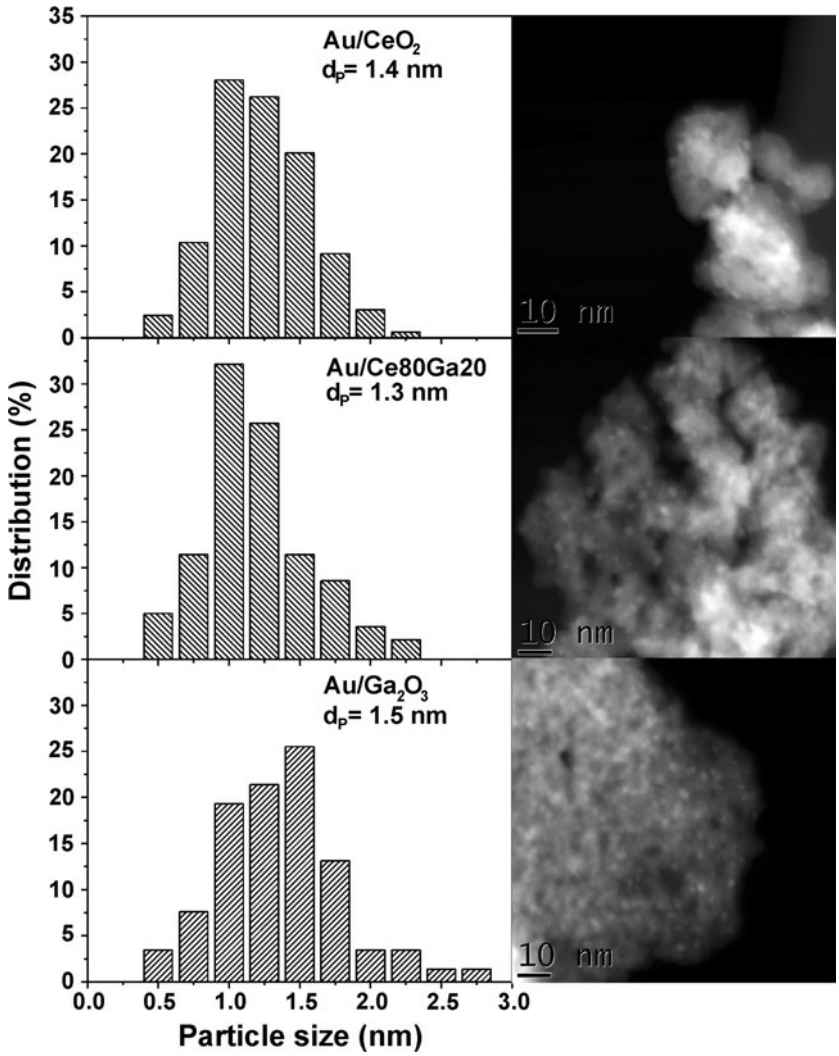

Fig. 5 Gold particle size distributions obtained by HAADF-STEM, of supported-gold on cerium, gallium, and cerium–gallium oxides after the oxidizing treatment in 5% O_2/He at 250 °C (1 h). Representative HAADF-STEM images are shown on the right side

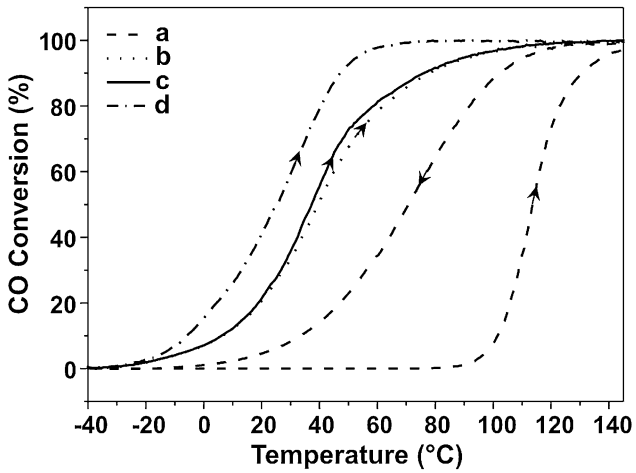

Fig. 6 Light-off curves for CO oxidation as a function of the activation pre-treatment on Au/Ce80Ga20: (*a*) without pretreatment, (*b*) reduction, H_2 (5%) at 200 °C (1 h), (*c*) oxidation, O_2 (5%) at 250 °C (1 h), followed by H_2 reduction (5%) at 200 °C (1 h), (*d*) oxidation, O_2 (5%) at 250 °C (1 h). The *arrows* indicate heating (*up*) or cooling (*down*) ramp

3.2.2 CO Oxidation

Figure 7 shows the light-off curves of the CO oxidation over the whole set of catalysts studied during the heating and cooling ramps between −40 and 145 °C. The light-off temperatures for both ramps are summarized in Table 2, together with the values reported for other widely studied gold catalysts [14].

The catalysts prepared in this study were very active towards CO oxidation during the heating ramp. They showed CO conversions (that is, T_{50}) equivalent to a Au/Ce68Zr32 catalyst, which has a gold loading of 3% wt/wt. Moreover, those cerium based catalysts were even more active than the reference catalyst Au/TiO_2 [24], during both ramp of temperature (Table 2).

In all cases, the light-off temperatures during the cooling ramp were always higher than the one during the heating processes. These hysteresis loops indicate that the supported Au catalysts have suffered some degree of

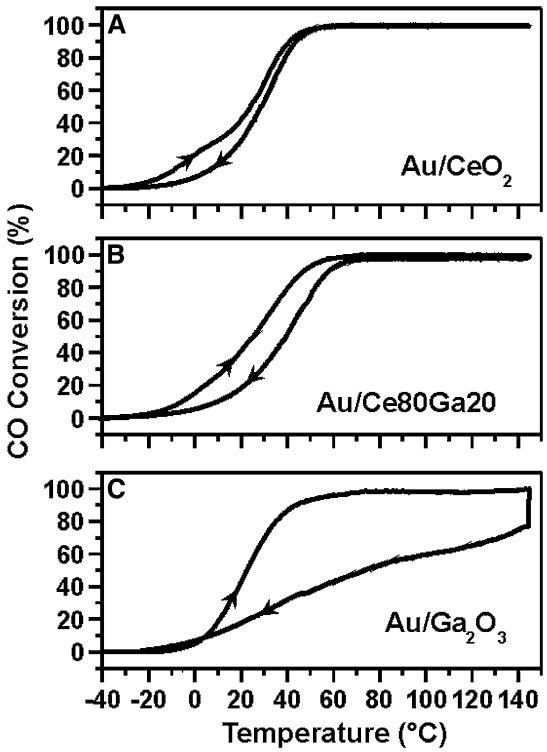

Fig. 7 Light-off curves for CO oxidation using the following catalysts: **a** $AuCeO_2$, **b** Au/Ce80Ga20, and **c** Au/Ga_2O_3. Reaction conditions: 1% CO + 0.6% O_2 balanced with He (total flow = 100 mL/min), 25 mg of catalyst. The *arrows* indicate heating (*up*) or cooling (*down*) ramp

deactivation, but the nature of their behaviors was different in each case.

The Au/CeO_2 catalyst initially deactivates during the heating ramp where a change of light-off curve slope at approximately 0 °C is observed (Fig. 7a). Afterwards, its activity remains virtually identical during the increasing and decreasing of temperature (the difference between the light-off temperatures during the cooling and heating ramps, ΔT_{50}, is 5 °C—see Table 2). The Au/Ce80Ga20 and Au/Ga_2O_3 catalysts showed ΔT_{50} values equal to 15 and 52 °C, respectively, indicating a more remarkable deactivation for the latter catalyst (see Fig. 7c).

To understand the origin of such deactivations, the size distribution of gold particles was measured by TEM for each catalyst at the end of the oxidation process. Table 2 summarizes the post-reaction Au dispersions calculated from the average size of supported Au crystallites.

It seems to be a clear correlation between the stability of the supported gold catalysts and the gold dispersion variation. The Au/CeO_2 catalyst showed the greatest stability, and the metal dispersion slightly decreased from 68 to 57%. However, the Au/Ga_2O_3 catalyst showed the highest deactivation, which was accompanied by the most pronounced drop of gold dispersion from 68 to 27%. Finally, the Au/Ce80Ga20 catalyst presented an intermediate behavior for both stability and change in metal dispersion, as compare to the previous catalyst.

Therefore, it is suggested that the presence of gallium, at least for a 20% at/at composition, has a deleterious effect on the stability of Au nanoparticles anchored to the support. Thus, gallium seems to favor the sintering of gold particles under CO oxidation reaction conditions.

3.2.3 *Water Gas Shift Reaction*

The performance of the catalysts for the WGS reaction was also investigated under pseudo steady state conditions at different reaction temperatures. Figure 8 shows the CO conversion versus the temperature of the reaction.

The Au catalyst supported on Ga_2O_3 presents a very low conversion over the whole temperature range, reaching only a 10% of CO conversion at 350 °C. Au/CeO_2 catalyst displayed the highest activity, which is similar to that reported by Leppelt et al. [25]. In this last case, conversion values of the thermodynamic equilibrium were achieved from 250 °C (T_{50} = 160 °C). On the other hand, the Au/Ce80Ga20 catalyst showed intermediate values of activity as compare to the gold catalyst supported on the pure oxides.

Table 2 Pre- and post-reaction gold dispersion (D) and light-off temperature (T_{50}) for the oxidation of CO

Catalyst	Au loading (% wt/wt)	D[a]		T_{50}		References
		Pre-reaction (%)	Post-reaction (%)	Heating ramp (°C)	Cooling ramp (°C)	
Au/CeO_2	2	68	57	24	29	This work
Au/Ga_2O_3	2	62	27	22	74	This work
Au/Ce80Ga20	2	67	40	25	40	This work
Au/Ce68Zr32[b]	3	53	–	28	38	[23]
Au/TiO_2	1.5	30	–	48	64	[24]

Reaction mixture: 1% CO + 0.6% O_2 balanced with He (total flow = 100 mL/min), 25 mg of catalyst

[a] Gold dispersion was calculated as described in [22]

[b] Stoichiometric composition: $Ce_{0.68}Zr_{0.32}O_2$

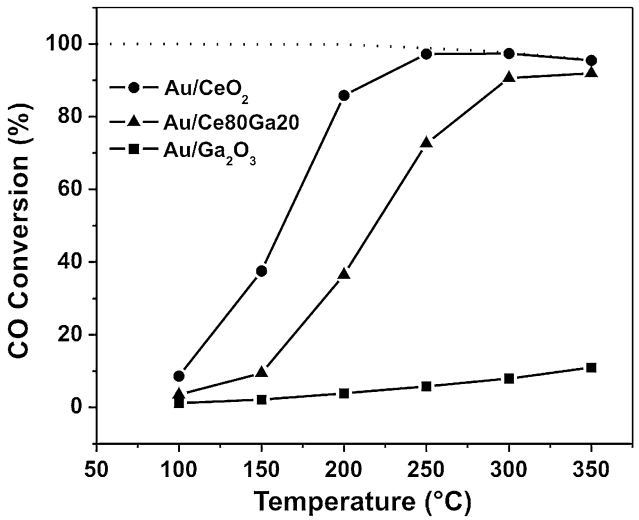

Fig. 8 CO conversion as a function of temperature for the WGS reaction. Catalysts: Au/CeO_2, Au/Ga_2O_3 and Au/Ce80Ga20. Reaction Conditions: 1% CO + 1.9% H_2O balanced with He (total flow = 100 mL/min), 50 mg of catalyst. *Dotted line* indicates the CO thermodynamic equilibrium conversion

It has been claimed that the WGS reaction on gold-based catalysts proceeds via the formation of carbonate or carboxylate species that change to formate species (associative mechanism) and eventually at higher temperatures to the oxidation-reduction of the support (redox mechanism), which takes place near the interface gold-support [14, 25–27]. In the first mechanism, it is suggested that the formate groups are decompose by water. In the last mechanism, the reduction of the support by the CO, previously adsorbed on Au sites, is proposed, followed by the support re-oxidation by water. The nature of the active form of gold (metal or ion), and the role of the support in its stabilization, have been a matter of debate [26]. However, measurements by in situ X-ray absorption spectroscopy indicate that $Au^{\delta+}$ species are not stable under WGS conditions [26, 28].

Thus, under the redox mechanism, the low activity shown by the Au/Ga_2O_3 catalyst can be explained on the basis of the poor reducibility of the support as shown by the TPR-CO trace in Fig. 4 for the gallia support.

However, there is not a direct explanation for the lower activity towards the WGS reaction after the Ga^{3+} incorporation to the structure of CeO_2, since the TPR-CO trace for Ce80Ga20 shows higher reducibility than ceria (Fig. 3). In other words, the highest degree of reducibility of Ce–Ga mixed oxide compared to that of pure ceria does not seem to be the determining factor of the lower activity of Au/Ce80Ga20 against Au/CeO_2.

As one point of view, it has been postulated that surface carboxylates or carbonates species can be responsible for catalytic deactivation of Au/support, especially when the catalyst is subjected to frequent shut-down/start-up operations [29–31]. Preliminary characterization studies of the supports showed that the cerium–gallium mixed oxide is able to form less carbonate species and the stability of these surface species is lower that on pure ceria [17]. Thus, we can conclude that the lower basicity of the Ce80Ga20 support is not enough to improve the activity and stability to the WGS reaction of supported gold catalyst.

On the other hand, there are at least two additional aspects to be considered. First, and as mentioned above, the redox mechanism suggests that water is needed to re-oxidize surface Ce^{3+}, that is, to quench oxygen vacancies of the support. Hence, the greater degree of reducibility of Ce80Ga20 versus CeO_2 does not imply a greater capacity of re-oxidation of the support by water. Moreover, a careful analysis of the redox properties at low temperature of the gold catalysts would be necessary to establish an appropriate correlation between redox and catalytic properties, as was highlighted for the Cu–Ce–Tb–O system using TPR-CO and infrared spectroscopy (IR) experiments [32]. Second, the results reported here of CO oxidation showed that the sintering of gold particles was more pronounced in the supports containing gallium. It is suggested then, that the more severe reaction conditions employed for the WGS reaction as compare to those used during the light-off curves of CO oxidation (that is, higher temperatures, longer reaction times and the presence of water), may have had a more pronounced effect on the sintering of gold particles supported on Ce80Ga20 than on CeO_2. Then, future studies of the oxygen storage capacity, TPR-CO combined with IR, and transmission electron microscopy will clarify which of these aspects may have (greater) impact on the different catalytic performance of the WGS reaction on these cerium based catalyst.

4 Conclusions

The nanostructural analysis of a cerium–gallium mixed oxide support, with a Ce-to-Ga atomic composition equal to 80/20 (named Ce80Ga20), shows that gallium cations are incorporated homogeneously into the fluorite type structure of ceria, and that Ce80Ga20 material has an enhanced reducibility as compared to pure ceria.

Highly dispersed gold catalysts were synthesized (2% wt/wt) by the deposition-precipitation method with urea over ceria, gallia and mixed cerium–gallium oxide supports. The Au particles size distributions were narrow, with an average particle diameter equal to 1.5 nm.

Supported Au catalysts showed a high initial activity for CO oxidation. However, these catalytic systems lost activity under reaction conditions. The order of stability was: $Au/CeO_2 > Au/Ce20Ga80 \gg Au/Ga_2O_3$. The gold

dispersion notoriously decreased on the gallium containing catalysts after the CO oxidation tests, and that deactivation was correlated to this dispersion variation.

The order of catalytic activity for the WGS reaction was: $Au/CeO_2 > Au/Ce80Ga20 \gg Au/Ga_2O_3$. If a redox mechanism is assumed, the low activity to the WGS on Au/Ga_2O_3 can partially explained by the poor reducibility of the support. However, this support requirement is not enough to understand the lower activity on Au/Ce80Ga20 as compare to Au/CeO_2. Then, it is necessary to explore other factors such as oxygen storage capacity of the supports and the degree of metal sintering to elucidate the difference between the catalytic behaviors of gold cerium-based catalysts.

Acknowledgments This work was supported by the ANPCyT of Argentina (PICT 2005 14-33101), the UNL (CAID 2009 J379), the MCINN of Spain/FEDER-EU (MAT2008/00889-NAN) and the Spanish International Cooperation Agency (PCI-AECID, Project A/9621/07, and A/18129/08). J.V. thanks the CONICET of Argentina for the grant received to carry out this work.

References

1. Barreto L, Makihira A, Riahi K (2003) Int J Hydrog Energy 28:267; and reference therein
2. van Santen RA (1999) Chapter 3: Fuel cells. In: Janssen FJJG, van Santen RA (eds) Environmental catalysis. Imperial College Press, London
3. Olah GA (2003, September 22) Chem Eng News, p 5
4. Olah GA (2004) Catal Lett 93:1
5. Carrette L, Friedrich KA, Stimming U (2001) Fuel Cells 1:5
6. Ghenciu AF (2002) Curr Opin Solid State Mater Sci 6:389
7. Thompson DT (2002) Nanotoday 2:40
8. Haruta M, Kobayashi T, Sano H, Yamada N (1987) Chem Lett 2:405
9. Haruta M, Kobayashi T, Iijim S, Delannay F (1988) In: Proceedings of the 9th international congress on catalysis, Calgary, Canada, p 1206
10. Haruta M, Saika K, Kobayashi T, Tsubota S, Nakahara Y (1988) Chem Express 3:159
11. Cosandey F, Madey TE (2001) Surf Rev Lett 8:73
12. Bamwenda GR, Tsubota S, Nakamura T, Haruta M (1997) Catal Lett 44:83
13. Valden M, Lai X, Goodman DW (1998) Science 281:1647
14. Bond GC, Louis C, Thompson DT (2006) Catalysis by gold. Catalytic science series, vol 6. World Scientific Publishing, London
15. Concepción P, Carrettin S, Corma A (2006) Appl Catal A 307:42
16. Deng W, Flytzani-Stephanopoulos M (2006) Angew Chem Int Ed 45:2285
17. Collins S, Finos G, del Río E, Alcántara R, Bernal S, Bonivardi A (2010) Appl Catal A 388:202
18. Collins SE, Baltanás MA, Bonivardi AL (2005) Langmuir 21:962
19. Zanella R, Giorgio S, Henry CR, Louis C (2002) J Phys Chem B 106:7634
20. Zanella R, Delannoy L, Louis C (2005) Appl Catal A 291:62
21. Zanella R, Giorgio S, Shin C, Henry CR, Louis C (2004) J Catal 222:357
22. López-Haro M, Delgado JJ, Cies JM, del Río E, Bernal S, Burch R, Cauqui MA, Trasobares S, Pérez-Omil JA, Bayle-Guillemaud P, Calvino JJ (2010) Angew Chem Int Ed 49:1981
23. Collins SE, Cies JM, del Río E, López-Haro M, Trasobares S, Calvino JJ, Pintado JM, Bernal S (2007) J Phys Chem C 111:14371
24. Reference catalyst provided by the World Gold Council, Lot: Au-T102 #02-6
25. Leppelt R, Schumacher B, Plzak V, Kinne M, Behm RJ (2006) J Catal 244:137
26. Burch R (2006) Phys Chem Chem Phys 8:5483
27. Senanayake SD, Stacchiola D, Evans J, Estrella M, Barrio L, Pérez M, Hrbek J, Rodríguez JA (2010) J Catal 271:392
28. Wang X, Rodríguez JA, Hanson JC, Pérez M, Evans J (2005) J Chem Phys 123:221101
29. Abd El-Moemen A, Karpenko A, Denkwitz Y, Behm RJ (2009) J Power Sources 190:64
30. Karpenko A, Leppelt R, Cai J, Plzak V, Chuvilin A, Kaiser U, Behm RJ (2007) J Catal 250:139
31. Fu Q, Deng W, Saltsburg H, Flytzani-Stephanopoulos M (2005) Appl Catal B 56:57
32. Hornés A, Bera P, López Cámara A, Gamarra D, Munuera G, Matínez-Arias A (2009) J Catal 268:367